

## VU Research Portal

### Laboratory measurements and T-matrix calculations of the scattering matrix of rutile particles in water

Volten, H.; Jalava, J.-P.; Lumme, K.; de Haan, J.F.; Vassen, W.; Hovenier, J.W.

**published in**

Applied Optics  
1999

**DOI (link to publisher)**

[10.1364/AO.38.005232](https://doi.org/10.1364/AO.38.005232)

**document version**

Publisher's PDF, also known as Version of record

[Link to publication in VU Research Portal](#)

**citation for published version (APA)**

Volten, H., Jalava, J.-P., Lumme, K., de Haan, J. F., Vassen, W., & Hovenier, J. W. (1999). Laboratory measurements and T-matrix calculations of the scattering matrix of rutile particles in water. *Applied Optics*, 38(24), 5232-5240. <https://doi.org/10.1364/AO.38.005232>

**General rights**

Copyright and moral rights for the publications made accessible in the public portal are retained by the authors and/or other copyright owners and it is a condition of accessing publications that users recognise and abide by the legal requirements associated with these rights.

- Users may download and print one copy of any publication from the public portal for the purpose of private study or research.
- You may not further distribute the material or use it for any profit-making activity or commercial gain
- You may freely distribute the URL identifying the publication in the public portal ?

**Take down policy**

If you believe that this document breaches copyright please contact us providing details, and we will remove access to the work immediately and investigate your claim.

**E-mail address:**

[vuresearchportal.ub@vu.nl](mailto:vuresearchportal.ub@vu.nl)

# Laboratory measurements and T-matrix calculations of the scattering matrix of rutile particles in water

Hester Volten, Juho-Pertti Jalava, Kari Lumme, Johan F. de Haan, Wim Vassen, and Joop W. Hovenier

We present experimentally determined scattering matrix elements of birefringent rutile particles in water as a function of the scattering angle for a wavelength of 633 nm (in air). These elements are compared with the results of T-matrix calculations for prolate spheroids. For the diagonal matrix elements the results of the T-matrix calculations are in good agreement with those of the measurements. A good fit for the whole matrix, including the off-diagonal elements, is obtained when we compensate for the birefringence of the rutile particles by performing the computations for spheroids with a slightly larger length/width ratio than measured. © 1999 Optical Society of America

*OCIS codes:* 290.0290, 120.5410.

## 1. Introduction

The optical behavior of rutile (titanium dioxide) particles is of considerable interest for two reasons. First, rutile pigments, consisting of small rutile particles, are widely employed in industry as constituents of paints, plastics, printing inks, and papers. These pigments are used for their extreme whiteness, high opacity, and high tinting strength.<sup>1</sup> Second, the large birefringence of the rutile particles is of particular interest from a theoretical point of view.<sup>2,3</sup>

The optical properties of rutile pigments depend on the light-scattering and the absorption behavior of constituent rutile particles. Since pure rutile particles are transparent at visible wavelengths, absorption by the sample particles is due to trace elements such as chromium<sup>4</sup> and will generally be small. In contrast, scattering by rutile particles is very strong in the visible part of the spectrum because of the

large real parts of the refractive index for their ordinary and extraordinary axes. Other properties that determine the scattering behavior are the particle shape and orientation, the size distribution of the particles, the distances between the particles, and the wavelength of the light used.

To determine theoretically the optical properties of rutile pigments, it is necessary to know the single-scattering behavior of the particles in the pigments, specifically their scattering matrix. It is not trivial to obtain accurately the scattering matrix of an ensemble of rutile particles in random orientation, either experimentally or numerically. These particles have a strong tendency to form aggregates in air, but their optical properties can be measured when these particles are suspended in water. However, the air-glass-water interface of, for example, a glass cuvette filled with such a suspension produces unwanted reflections that complicate the measurements as well as the data reduction.<sup>5,6</sup> This makes it difficult, time-consuming, and costly to do these measurements on a regular basis, e.g., during the manufacturing process. On the other hand, numerical calculations of scattering matrices of ensembles of rutile particles tend to be rather difficult and computer time-consuming because of the birefringence and the complex crystal shape of the particles whereas simplification of the calculation method requires validation.

In this paper we present results of laboratory measurements of the scattering matrix elements as a function of the scattering angle for rutile particles in water for a wavelength of 633 nm (in air). To cali-

---

H. Volten, J. F. de Haan, W. Vassen, and J. W. Hovenier are with the Department of Physics and Astronomy, Free University, De Boelelaan 1081, NL-1081 HV Amsterdam, The Netherlands. J. W. Hovenier is also with the Astronomical Institute "Anton Pannekoek," University of Amsterdam, Kruislaan 403, NL-1098 SJ Amsterdam, The Netherlands. J.-P. Jalava is with Kemira Pigments Oy, FIN-28840 Pori, Finland. K. Lumme is with the Observatory, P.O. Box 14, University of Helsinki, FIN-00014 Helsinki, Finland. The e-mail address for H. Volten is hester@nat.vu.nl.

Received 10 March 1999; revised manuscript received 26 May 1999.

0003-6935/99/245232-09\$15.00/0

© 1999 Optical Society of America

brate our setup, we use the results of measurements on latex spheres, because they can be compared with the results of (exact) Mie calculations. We investigate the extent to which results of relatively fast and easily implemented T-matrix calculations<sup>7</sup> can be used to describe the scattering behavior of the rutile particles. For these T-matrix calculations the somewhat prolate rutile particles are approximated by prolate spheroids and the birefringence of the particles is neglected. Comparison of the results of the rutile particles measurements, on the one hand, and results of these T-matrix calculations, on the other hand, reveals the accuracy of these approximations for a theoretical determination of optical scattering properties of rutile particles.

## 2. Some Concepts from Light-Scattering Theory

We briefly summarize some concepts of light-scattering theory. The energy flux and polarization of a beam of light can be represented by a column vector  $\mathbf{I} = \{I, Q, U, V\}$ , the Stokes vector.<sup>2,8</sup> The Stokes parameter  $I$  is proportional to the total energy flux of the beam. Stokes parameters  $Q$  and  $U$  represent the differences between two components of the flux for which the electric-field vectors oscillate in orthogonal directions. The Stokes parameter  $V$  is the difference between two oppositely circularly polarized components of the flux.

If, as in our experiment, light is scattered by an ensemble of randomly oriented particles and reciprocity applies, the Stokes vectors of the incident beam and the scattered beam are, for each scattering angle  $\theta$ , related by a  $(4 \times 4)$  scattering matrix<sup>2</sup>:

$$\begin{pmatrix} I_s \\ Q_s \\ U_s \\ V_s \end{pmatrix} = \frac{\lambda^2}{4\pi^2 D^2} \begin{pmatrix} F_{11} & F_{12} & F_{13} & F_{14} \\ F_{12} & F_{22} & F_{23} & F_{24} \\ -F_{13} & -F_{23} & F_{33} & F_{34} \\ F_{14} & F_{24} & -F_{34} & F_{44} \end{pmatrix} \begin{pmatrix} I_i \\ Q_i \\ U_i \\ V_i \end{pmatrix}. \quad (1)$$

Here subscript  $s$  is the scattered beam, subscript  $i$  is the incident beam,  $\lambda$  is the wavelength, and  $D$  is the distance from the scatterers to the detector. In this case the scattering matrix elements are independent of the azimuthal angle. The plane through the direction of propagation of the incident and the scattered light beams is chosen as a plane of reference, the scattering plane.

The elements of the scattering matrix contain information about the size, shape, and refractive index of the scatterers. It contains 10 independent matrix elements that have to be determined. For convenience we normalize all matrix elements to  $F_{11}$ ; i.e., we present results for  $F_{11}$  and  $F_{ij}/F_{11}$  with  $i, j = 1-4$ . Note that  $|F_{ij}/F_{11}| \leq 1$ .<sup>9</sup> A stricter test for the relationships between matrix elements is formed by the Cloude coherency test as described by Hovenier and van der Mee.<sup>10</sup> For all the measurements reported in this paper, we have investigated the reliability of the measured angular distributions by applying this Cloude coherency test; i.e., we checked to determine whether each measured matrix can be a sum of pure

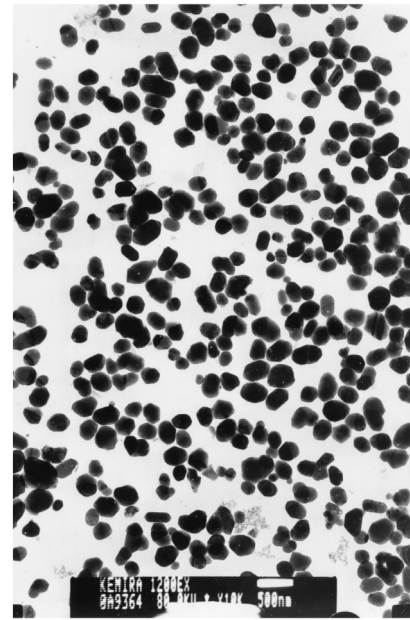


Fig. 1. TEM image of rutile particles. The white bar at the bottom of the image denotes 500 nm.

scattering matrices. In all cases this test was satisfied within the limits of the error bars.

## 3. Properties of the Rutile Particles

Rutile particles are birefringent, the real part of the refractive index  $n$  at 633 nm is 2.872 (2.156 relative to water) for the extraordinary and 2.584 (1.940 relative to water) for the ordinary axis.<sup>11</sup> The refractive index of water at 633 nm is 1.332.<sup>12</sup> The sample that we used consisted of a water suspension of pure, uncoated rutile particles with a small (0.2%) amount of dispersing agent. The rutile particles were prepared by the so-called sulfate process at Kemira Pigments Oy, Pori, Finland. In Fig. 1 a transmission-electron-microscope image of rutile particles is displayed. From mineralogy it is known that rutile crystals have two axes of the same length, while the third axis is generally the longest. Therefore most rutile particles tend to have a prolate shape. This is consistent with the shapes in Fig. 1, if we assume that the particles are randomly orientated. The particle size and the shape were measured as width and length/width distributions by using transmission electron microscopy<sup>13</sup> (TEM) (Jeol Jem 1200 EX, calibrated with latex spheres) and are shown by solid curves in Fig. 2. The dashed curves in Fig. 2 are discussed in Section 7. Expressed as a volume-equivalent sphere value, the diameter  $d_{\text{TEM}}$  of the rutile particles becomes 221(3) nm with a standard deviation  $\sigma_{\text{TEM}}$  of 57(3) nm. The digits within parentheses represent the uncertainty in the last digits of the given values.

## 4. Experimental Setup

The scattering matrix of the rutile particles has been measured with the experimental setup developed at

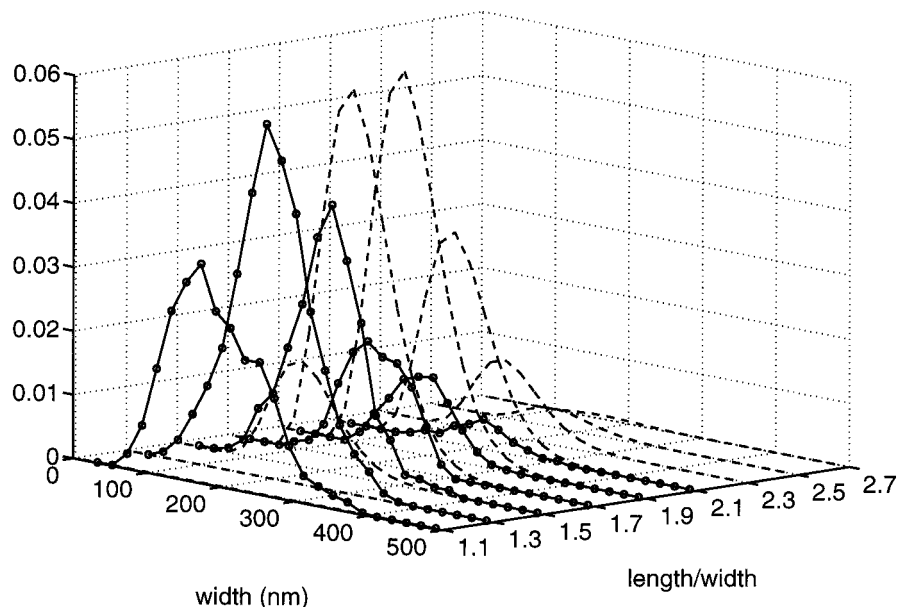


Fig. 2. Two-dimensional distribution of the width and the length/width of the rutile sample. The normalization is such that the sum of all values for 180 combinations of width and length/width equals unity. Solid curves, values determined by TEM; dashed curves, estimated values obtained by fitting results of the T-matrix calculations to measured angular distributions of scattering matrix elements (see Section 7).

the Department of Physics and Astronomy of the Free University in Amsterdam.<sup>14</sup> This setup was originally designed to determine the scattering matrix of aerosol particles.<sup>15–17</sup> However, the setup was adapted for measuring particles in water.<sup>6</sup>

A schematic of the experimental setup is shown in Fig. 3. Light with a wavelength of 633 nm from a continuous-wave He–Ne laser passes through a polarizer oriented at an angle  $\gamma_P$  and an electro-optic modulator oriented at an angle  $\gamma_M$ . The orientation angles of optical elements are measured counterclockwise from the scattering plane when one is looking in the direction of propagation of the light. The modulated light is subsequently scattered by the sample of rutile particles. The scattered light passes through a quarter-wave plate oriented at an

angle  $\gamma_Q$  and an analyzer oriented at an angle  $\gamma_A$  (both optional) and is detected by a photomultiplier tube that moves along a ring. The detector covers a scattering angle range from 15 deg (nearly forward scattering) to 165 deg (nearly backward scattering).

The modulator in the setup in combination with lock-in detection increases the accuracy of the measurements and makes it possible to deduce several elements of the scattering matrix from one detected signal. A voltage varying sinusoidally in time is applied to the modulator crystal. The phase shift caused by the crystal is also sinusoidal, so that the resulting phase shift can be described by Bessel functions of the first kind  $J_k(x)$ . If the amplitude  $\phi_0$  of the varying phase shift is chosen appropriately, the flux reaching the detector is<sup>14</sup>

$$I_{\text{det}}(\theta) = c[DC(\theta) + 2J_1(\phi_0)S(\theta)\sin \omega t + 2J_2(\phi_0)C(\theta)\cos 2\omega t + \dots], \quad (2)$$

where  $J_1(\phi_0)$  and  $J_2(\phi_0)$  are known constants and  $c$  is a constant for a certain optical arrangement. The modulation frequency  $\omega$  is 1 kHz. The coefficients  $DC(\theta)$ ,  $S(\theta)$ , and  $C(\theta)$  contain elements of the scattering matrix (see Table 1; e.g., Refs. 14 and 17). By using lock-in detection the dc,  $\sin \omega t$ , and  $\cos 2\omega t$  terms containing, respectively,  $DC(\theta)$ ,  $S(\theta)$ , and  $C(\theta)$  are separated. The  $\sin \omega t$  and  $\cos 2\omega t$  parts are subsequently divided by the dc part of the signal belonging to the same configuration, which for these ratios eliminates the constant  $c$ . Note that  $F_{11}(\theta)$  is obtained only on a relative scale in our experiments. Finally, when  $F_{12}/F_{11}$ ,  $F_{13}/F_{11}$ , and  $F_{14}/F_{11}$  measured with combinations 1 and 5 in Table 1 are used, other element ratios  $F_{ij}/F_{11}$  are extracted from the

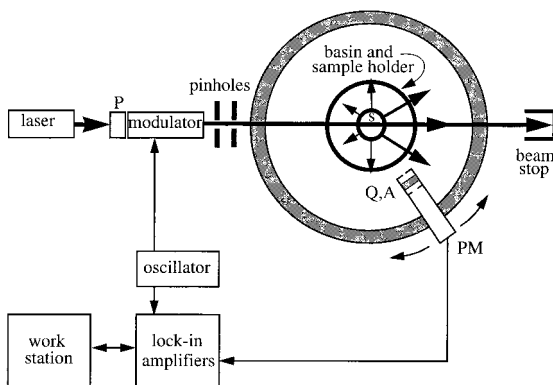


Fig. 3. Schematic of the experimental setup: P, polarizer; S, rutile sample in water; PM, photomultiplier; A, (optional) analyzer; Q, (optional) quarter-wave plate. The photomultipliers are mounted on a goniometer ring with an outer diameter of 1 m.

**Table 1. Matrix Elements Measured for Eight Combinations of the Orientation Angles  $\gamma_P$ ,  $\gamma_M$ ,  $\gamma_Q$ , and  $\gamma_A$  of the Polarizer, the Modulator, the Quarter-Wave Plate, and the Analyzer<sup>a</sup>**

Combination	$\gamma_P$ (deg)	$\gamma_M$ (deg)	$\gamma_Q$ (deg)	$\gamma_A$ (deg)	$DC(\theta)$	$S(\theta)$	$C(\theta)$
1	0	-45	-	-	$F_{11}$	$-F_{14}$	$F_{12}$
2	0	-45	-	0	$F_{11} + F_{12}$	$-(F_{14} + F_{24})$	$F_{12} + F_{22}$
3	0	-45	-	45	$F_{11} - F_{13}$	$-(F_{14} + F_{34})$	$F_{12} - F_{23}$
4	0	-45	0	45	$F_{11} + F_{14}$	$-(F_{14} + F_{44})$	$F_{12} + F_{24}$
5	45	0	-	-	$F_{11}$	$-F_{14}$	$F_{13}$
6	45	0	-	0	$F_{11} + F_{12}$	$-(F_{14} + F_{24})$	$F_{13} + F_{23}$
7	45	0	-	45	$F_{11} - F_{13}$	$-(F_{14} + F_{34})$	$F_{13} + F_{33}$
8	45	0	0	45	$F_{11} + F_{14}$	$-(F_{14} + F_{44})$	$F_{13} - F_{34}$

<sup>a</sup> $S(\theta)$  and  $C(\theta)$  are subsequently divided by the  $DC(\theta)$  output belonging to the same configuration.

ratios measured with combinations 2, 3, 4, 6, 7, and 8. For example, we find  $F_{24}/F_{11}$  from

$$\frac{F_{14} + F_{24}}{F_{11} + F_{12}} = \frac{F_{14}/F_{11} + F_{24}/F_{11}}{1 + F_{12}/F_{11}}, \quad (3)$$

since it is the only unknown ratio in Eq. (3). Other element ratios are extracted in a similar way.

The rutile sample is contained in a cylindrically shaped cuvette, 30 mm in diameter, made of Pyrex glass. A magnetic stirrer continuously homogenizes the sample. To reduce reflections of the incident light from the glass cuvette, one places the cuvette in the center of a cylindrical Pyrex glass basin (22 cm in diameter) filled with glycerin. Since glycerin has the same refractive index as glass ( $n = 1.5$ ), strong reflections take place farther from the scattering sample. Also, the glass basin has flat entrance and exit windows to prevent reflections of the incident laser beam on the basin from reaching the detectors as well as to avoid spherical aberrations of the incident beam. In spite of these precautions a small fraction of the light scattered by rutile particles is still reflected either by the wall of the cuvette or by the basin. In addition, a small fraction of the unscattered light is reflected by the wall of the cuvette or basin and can thereafter be partly scattered.<sup>5,18</sup> When reflections of the light on the wall of the cuvette or basin are assumed to be perpendicular and we take into account multiple reflections, we find the following exact equation for the true scattering matrix of the rutile particles (see also Ref. 6):

$$\mathbf{F}(\theta) = \mathbf{F}^{\text{unc}}(\theta) - [r\mathbf{R}\mathbf{F}^{\text{unc}}(180^\circ - \theta) + \mathbf{F}^{\text{unc}}(180^\circ - \theta)r\mathbf{R}], \quad (4)$$

where  $\mathbf{F}^{\text{unc}}$  represents the uncorrected measured matrix,  $r$  is a (constant) reflection coefficient, and  $\mathbf{R}$  is the Fresnel matrix for perpendicular reflection. An empirical value for  $r$  of  $0.012 \pm 0.001$  has been deduced by minimizing the difference between the results of measurements on latex spheres with the results of Mie calculations.

In single-scattering experiments it is essential to avoid multiple scattering.<sup>19,20</sup> Therefore the sample concentration must be low enough. On the other hand, the signal-to-noise ratio decreases for low concentrations. To determine the highest sample con-

centration to which single scattering applies, the following method has been adopted. The detector is placed at a fixed position at 15 deg. Subsequently, a series of measurements is made with increasing sample concentration. As long as the scattered flux is proportional to the hydrosol concentration, multiple scattering is assumed to be negligible. In this manner the optimal concentration has been determined. We verified that at this concentration the average distance between the particles is sufficiently large to make the particles independent scatterers and near-field effects negligible.<sup>21</sup>

The medium in which the rutile particles were suspended consisted of Baker analyzed high-performance liquid chromatography (HPLC) reagent (HPLC water) with a small amount of dispersing agent. The flux of light scattered by the cuvette filled with only this background medium has been measured for each combination in Table 1 and has been subtracted from the corresponding results of the rutile particles measurements. The effect of the background correction is maximal for the forward and backward directions.<sup>6,22</sup>

The scattering volume seen by the detector is determined by the scattering angle, by the geometry of the scattering volume inside the cuvette (length, 30 mm, width, 1 mm; i.e., twice the waist of the laser beam), by the distance to the photomultiplier (300 mm), and by the circular pinholes in front of the photomultiplier (one with a diameter of 5 mm directly in front and one with a diameter of 2 mm at a distance of 100 mm from the photomultiplier tube). By taking this geometry into account and by assuming that the width of the laser beam can be neglected, a correction function of the scattering angle has been derived by which the measured flux has to be multiplied to correct for the scattering volume as seen by the detector. This function equals  $\sin \theta$  for most of the angle range (see Fig. 4), i.e., roughly between 25 and 155 deg (e.g., Ref. 3, Section 13.2.1) and has been used to correct the measurements.

## 5. Measurements on Latex Spheres

We have validated the results obtained with the experimental setup by comparing the measurements on latex spheres with the Mie calculations<sup>23</sup> for spherical particles with a log-normal size distribution<sup>24</sup>

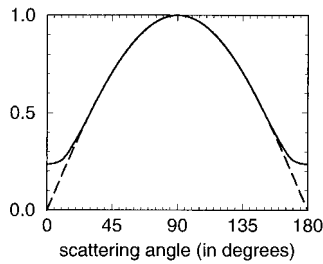


Fig. 4. Correction function of scattering angle (solid line) to correct the measured flux for the changing scattering volume as seen by the detector. This function equals  $\sin \theta$  (dashed curve) for most of the scattering angle range.

with  $r_{\text{eff}} = 0.2595 \mu\text{m}$ ,  $v_{\text{eff}} = 0.0057$ , and refractive index  $n + in' = 1.194 + i00$  relative to HPLC water. The values for  $r_{\text{eff}}$  and  $n + in'$  were specified by the manufacturer of the latex spheres (Duke Scientific Corporation). The value for  $v_{\text{eff}}$  was not specified and was therefore chosen so that the difference between the Mie calculations and the measurements was minimized by using a  $\chi^2$  method that took into consideration all the matrix elements. During this fitting procedure the normalization of the calculated

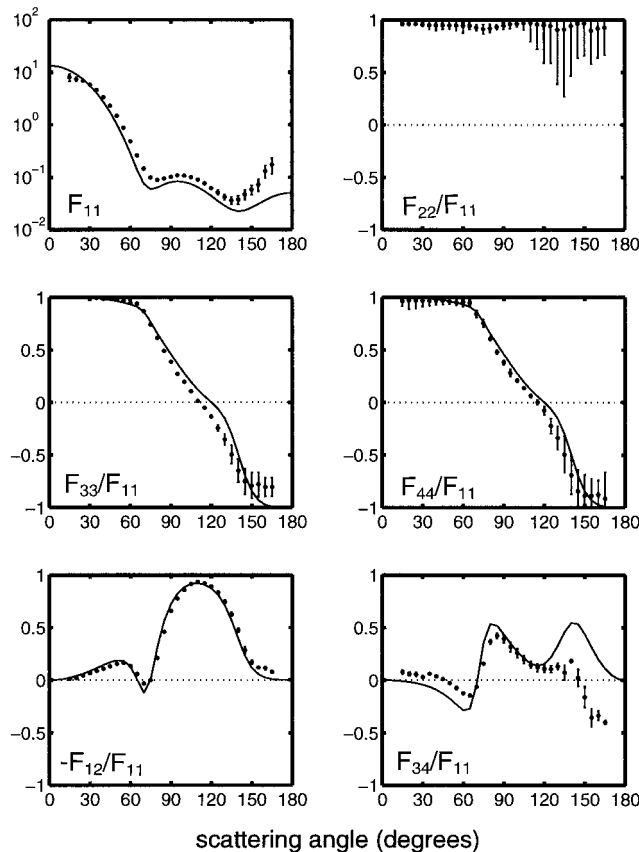


Fig. 5. Comparison of results of measurements on latex spheres in water (solid circles) with Mie calculations (solid curves) for angular distributions of  $F_{11}$ ,  $F_{22}/F_{11}$ ,  $F_{33}/F_{11}$ ,  $F_{44}/F_{11}$ ,  $-F_{12}/F_{11}$ , and  $F_{34}/F_{11}$ . Note that  $F_{11}$  is plotted on a log scale.

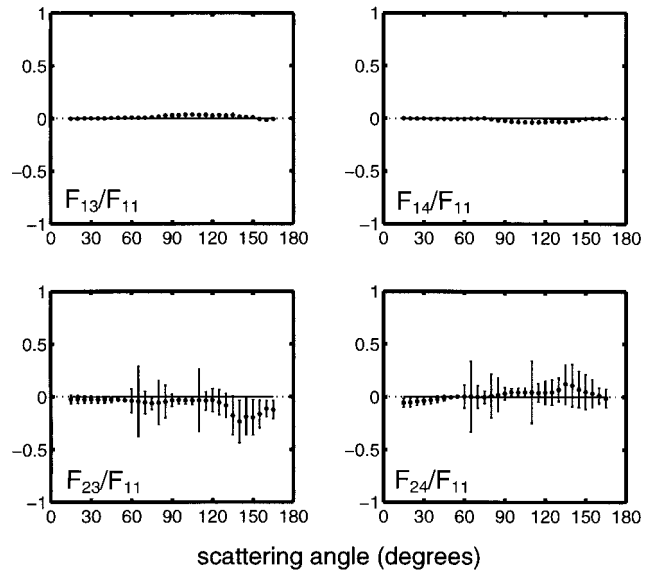


Fig. 6. Same as Fig. 5 but for  $F_{13}/F_{11}$ ,  $F_{14}/F_{11}$ ,  $F_{23}/F_{11}$ , and  $F_{24}/F_{11}$ .

$F_{11}(\theta)$  was chosen so that its average overall directions equals unity, i.e.,

$$\frac{1}{2} \int_0^\pi F_{11}(\theta) \sin \theta d\theta = 1, \quad (5)$$

and the normalization of the measured  $F_{11}(\theta)$  was chosen so that  $\chi^2$  was minimal.

The results of the measurements and calculations for all ten relevant matrix elements or element ratios are plotted as a function of scattering angle in Figs. 5 and 6. The error bars reflect the combined effect of errors due to (1) statistical variation in the measurements, (2) statistical variation in the background measurements, and (3) uncertainties in the determination of the reflection coefficient  $r$ .<sup>6</sup> If no error bar is indicated, the error is smaller than the symbol plotted.

When comparing the measurement results of the latex spheres with those of Mie calculations (see Figs. 5 and 6), we see that agreement for the shapes of the  $F_{11}(\theta)$  functions is good between 35 and 140 deg. For smaller angles, from 15 to 30 deg, the measured function is more shallow than the results of the Mie calculations, whereas for large angles, from approximately 140 to 165, the measured function curves upward at a significantly steeper angle. For the element ratios  $-F_{12}(\theta)/F_{11}(\theta)$  and  $F_{22}(\theta)/F_{11}(\theta)$  the agreement is good over the entire angle range measured.

Both  $F_{33}(\theta)/F_{11}(\theta)$  and  $F_{44}(\theta)/F_{11}(\theta)$ , which should be equal to each other according to Mie theory, agree well with the results of calculations except at large scattering angles where the measured values are somewhat higher than the calculated values. The measured element ratio  $F_{34}(\theta)/F_{11}(\theta)$  deviates considerably from the calculated one, although their behavior is similar.

Interestingly, Miller *et al.*<sup>25</sup> reported similar deviations for their calibration measurements on latex spheres of the same size obtained from the same manufacturer (Duke Scientific Corporation), in particular for  $F_{34}(\theta)/F_{11}(\theta)$ . This seems to indicate that either the particles do not completely obey Mie scattering or the specifications of the manufacturer are not accurate enough (see also Ref. 26). The measured element ratios  $F_{13}(\theta)/F_{11}(\theta)$ ,  $F_{14}(\theta)/F_{11}(\theta)$ ,  $F_{23}(\theta)/F_{11}(\theta)$ , and  $F_{24}(\theta)/F_{11}(\theta)$  do not differ from zero by more than the error bars.

## 6. Measurements on Rutile Particles in Water

The complete scattering matrix of rutile particles in water measured as a function of scattering angle is shown by filled circles in Figs. 7 and 8. The phase function  $F_{11}(\theta)$  has been normalized according to Eq. (5) where we used a Legendre series expansion to define  $F_{11}(\theta)$  for angles not covered by measurements. The scales for  $F_{ij}(\theta)/F_{11}(\theta)$  range from +1 to -1. Error bars are determined in the same way as for the latex spheres. The error bars are smaller than for the latex spheres, especially for  $F_{22}(\theta)/F_{11}(\theta)$ , because rutile particles are much stronger scatterers than latex spheres particularly at side-scattering and backscattering angles. For example, the measured  $F_{11}(\theta)$  varies by no more than a factor of 17 over the covered angles. For the latex spheres it is a factor of 226.

As is clear from Fig. 7, the angular distribution of  $F_{22}(\theta)/F_{11}(\theta)$  of the rutile particles deviates significantly from one, ranging between approximately 0.6 and 1.0. The shapes of  $F_{33}(\theta)/F_{11}(\theta)$  and  $F_{44}(\theta)/F_{11}(\theta)$  are similar except at small angles where  $F_{44}(\theta)/F_{11}(\theta)$  is approximately 0.1 lower than  $F_{33}(\theta)/F_{11}(\theta)$  and at large angles where  $F_{44}(\theta)/F_{11}(\theta)$  is approximately 0.15 higher. Both ratios vanish at approximately the same angle (between 120 and 125 deg), as does  $F_{34}(\theta)/F_{11}(\theta)$ . The  $-F_{12}(\theta)/F_{11}(\theta)$  ratio peaks at  $\sim 75$  deg with a maximum value of 0.18 and is positive for most angles but becomes slightly negative beyond 140 deg.

The scattering-element ratio  $F_{24}(\theta)/F_{11}(\theta)$  in Fig. 8 deserves special attention because it deviates from zero by more than the error bars. This particular behavior is probably the result of the strong birefringence of the rutile particles, since for randomly oriented isotropic particles having a plane of symmetry  $F_{24}(\theta)/F_{11}(\theta)$  is identical to zero, just like  $F_{13}(\theta)/F_{11}(\theta)$ ,  $F_{14}(\theta)/F_{11}(\theta)$ , and  $F_{23}(\theta)/F_{11}(\theta)$ . For  $F_{23}(\theta)/F_{11}(\theta)$  we find no significant deviations from zero, and  $F_{13}(\theta)/F_{11}(\theta)$  as well as  $F_{14}(\theta)/F_{11}(\theta)$  is clearly zero at all angles within the experimental errors.

## 7. T-Matrix Calculations

The theoretical interpretation of light-scattering measurements of rutile particles is complicated for at least two reasons. First, rutile is a highly anisotropic, birefringent substance. Second, the shape of a typical rutile particle cannot be described precisely by a simple geometric figure.

We have chosen to apply the T-matrix method to

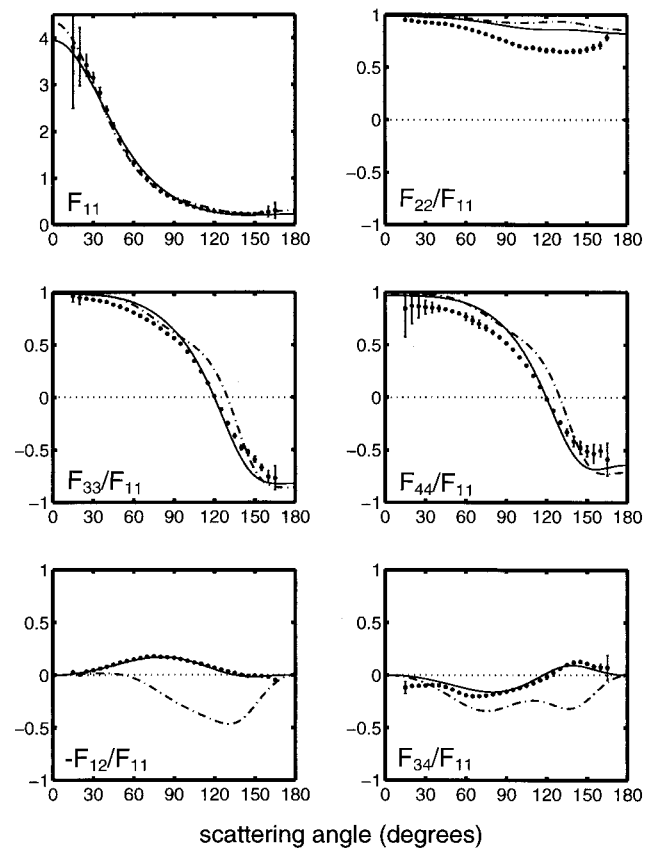


Fig. 7. Comparison of results of measurements on rutile particles in water with the results of T-matrix calculations for the angular distributions of  $F_{11}$ ,  $F_{22}/F_{11}$ ,  $F_{33}/F_{11}$ ,  $F_{44}/F_{11}$ ,  $-F_{12}/F_{11}$ , and  $F_{34}/F_{11}$ . The normalization of  $F_{11}(\theta)$  is such that its average over three-dimensional space equals unity. Solid circles, measured values, dash-dot curves, functions calculated with the T-matrix method by using the width and the length/width distributions determined by TEM (see Fig. 2 and Table 2); solid curves, the same but for estimated values obtained by fitting the results of T-matrix calculations to measured angular distributions of scattering matrix elements (see Fig. 2 and Table 2).

our measurements because it is fast and easy to implement. In doing this we adopt a prolate ellipsoid model for the shapes and ignore the large birefringence of the rutile particles. The scattering matrix of rutile particles has been calculated with the T-matrix algorithm developed by Mishchenko.<sup>7,27</sup> According to past experience the gamma distribution is a suitable distribution for describing both the width and the length/width distributions of the rutile particles.<sup>13</sup> Actually we found that the results of the calculations are not sensitive to the precise shape of the distributions, as is consistent with other observations.<sup>28</sup>

The parameters for applying the T-matrix method to the measurements by using gamma distributions are as follows:

the mean width  $d_w$  of the particles,  
the standard deviation  $\sigma_w$  of the width distribution,  
the mean length/width ratio  $l/w$  of the prolate ellipsoids,

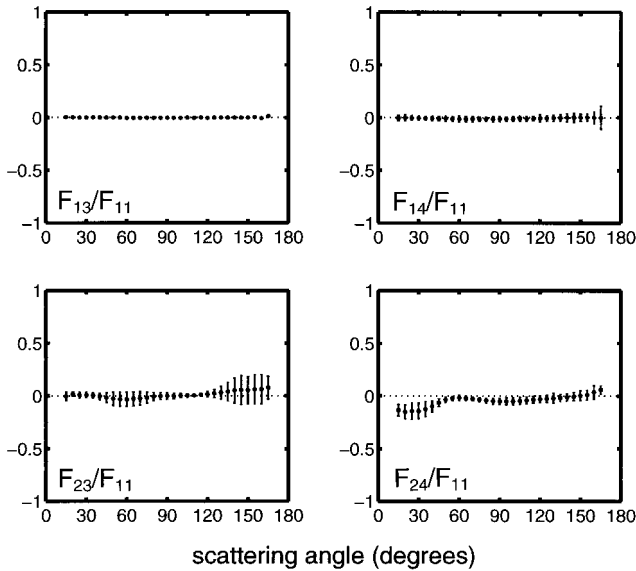


Fig. 8. Same as Fig. 7 but for  $F_{13}/F_{11}$ ,  $F_{14}/F_{11}$ ,  $F_{23}/F_{11}$ , and  $F_{24}/F_{11}$ . Results of calculations have been omitted for these element ratios since they are identically zero at all scattering angles.

the standard deviation  $\sigma_{l/w}$  of the length/width distribution, and the refractive index  $m = n + in'$ .

We performed a T-matrix calculation by using the values for the parameters measured with the TEM and an arithmetic mean of the literature values for the refractive indices (see Table 2). The results of this calculation are plotted in Fig. 7 as dash-dot curves where  $F_{11}(\theta)$  obeys Eq. (5). The agreement between the measured results and the results of the calculation is excellent for the shape of  $F_{11}(\theta)$ . For the other diagonal elements we find that the calculations provide a good reproduction of the trends seen for the measured results. However, a totally different behavior is found for two off-diagonal element ratios, namely,  $-F_{12}(\theta)/F_{11}(\theta)$  and  $F_{34}(\theta)/F_{11}(\theta)$ .

We have performed a least-squares fitting procedure to determine whether we can improve the comparison between measurements and calculations by

Table 2. Parameters Used in the T-Matrix Calculations Presented in Figs. 7 and 8<sup>a</sup>

Parameters	Measured	Estimated
$d_w$	198(4) nm	179 nm
$\sigma_w$	50(3) nm	45 nm
$l/w$	1.40(0.03)	1.88
$\sigma_{l/w}$	0.25(0.02)	0.23
$n + in'$	2.048 <sup>b</sup> + $i$ 0.00	1.986 + $i$ 0.00

<sup>a</sup>The measured particle size and shape distributions of the rutile particles have been determined with TEM. Estimated values were obtained by fitting the results of T-matrix calculations to measured angular distributions of scattering matrix elements. The digits within parentheses represent the uncertainties (one sigma standard deviations) of the given values.

<sup>b</sup>Average of the values 2.1562 and 1.9399 for the extraordinary and the ordinary axes, respectively.<sup>11</sup>

modifying the parameters slightly. We minimize the following sum of squares ( $SS$ ) with respect to the parameters mentioned above:

$$SS = SS1 + SS2 \quad (6)$$

with

$$SS1 = \frac{1}{N} \sum_{i=1}^N \left\{ [F_{11}(\theta_i)_{\text{meas}}/F_{11}(\theta_i)_{\text{calc}} - 1]^2 + \sum_j w_j [F_{j, \text{meas}}(\theta_i)/F_{11, \text{meas}}(\theta_i) - F_{j, \text{calc}}(\theta_i)/F_{11, \text{calc}}(\theta_i)]^2 \right\}, \quad (7)$$

$$SS2 = (d_{\text{TEM}} - d_{\text{calc}})^2 + (\sigma_{\text{TEM}} - \sigma_{\text{calc}})^2, \quad (8)$$

where  $j = 22, 33, 44, 12, 34$  and where meas and calc refer to the measured and the calculated values, respectively,  $N$  is the number of scattering angles, and  $w_j$  are the weights.  $F_{11}(\theta_i)_{\text{meas}}$  and  $F_{11}(\theta_i)_{\text{calc}}$  are normalized according to Eq. (5). The  $SS2$  term contains the volume-equivalent sphere diameters  $d_{\text{TEM}}$  and  $d_{\text{calc}}$  as well as the standard deviations  $\sigma_{\text{TEM}}$  and  $\sigma_{\text{calc}}$  derived from the TEM measurements and T-matrix calculations, respectively, expressed in nanometers. This term was added to constrain the combination of parameters  $d_w$  and  $l/w$  as well as  $\sigma_w$  and  $\sigma_{l/w}$ . In this way we ensured that the estimated width and the length/width distributions did not deviate too much from physical reality. We did the estimation by iterative least-squares minimization by using the Nelder Mead minimization algorithm that was implemented with Matlab and the Data Analysis Toolbox.<sup>29</sup> To obtain a solution in which the behavior of  $-F_{12}(\theta)/F_{11}(\theta)$  and  $F_{34}(\theta)/F_{11}(\theta)$  is emphasized, these terms were given a weight of 10; the other weights were one.

The results of the fit produced in this manner are shown in Fig. 7 by solid curves. The resulting estimated parameters are listed in Table 2. In addition the estimated width and length/width distributions are shown in a two-dimensional plot in Fig. 2 (dashed curves) to facilitate comparison with the measured ones. The volume-equivalent sphere diameter  $d_{\text{calc}}$  and the standard deviation  $\sigma_{\text{calc}}$  are equal to those determined with the TEM, i.e.,  $d_{\text{calc}} = 221$  nm and  $\sigma_{\text{calc}} = 57$  nm.

It is not entirely unexpected, because of the weights given to these functions, that the agreement between measured results and calculated functions has improved dramatically for  $-F_{12}(\theta)/F_{11}(\theta)$  and  $F_{34}(\theta)/F_{11}(\theta)$ . For the diagonal element ratios the agreement has also improved considerably, especially for  $F_{33}(\theta)/F_{11}(\theta)$  and  $F_{44}(\theta)/F_{11}(\theta)$  at side-scattering angles. A great difference is still present for  $F_{22}(\theta)/F_{11}(\theta)$ . It is likely that this element ratio is most sensitive to the actual shapes and birefringence of the rutile particles.

As can be seen in Table 2 and Fig. 2, the spheroids that produce the best fitted result are slightly nar-



rower and longer than the measured rutile particles. This is consistent with the fact that the best fitted refractive index (1.986) is smaller for the length and larger for the width than the real values of the rutile particles in water (2.1562 and 1.9399, respectively). The fits are virtually insensitive to the imaginary part  $n'$  when  $0 \leq n' \leq \sim 10^{-4}$ . The estimated standard deviations of the width and the length/width distributions are practically the same as those of the measured rutile particles.

## 8. Discussion

Interestingly, for the rutile particles  $F_{24}(\theta)/F_{11}(\theta)$  is nonzero over part of the angle range. This manifestation of anisotropy, which must be produced by the birefringence of the particles, cannot be reproduced by our T-matrix calculations, since, as we mentioned above, our calculations do not include birefringence. Hence the possibilities of modeling the measurements with these calculations are limited. Nevertheless, T-matrix calculations agree with the measured values reasonably well for several elements, for example, for the shape of  $F_{11}(\theta)$ . Even better results are obtained for the rutile particles with an estimated mean length/width value of 1.88, which is significantly larger than that determined with the TEM, i.e., length/width = 1.40(0.03). The estimated parameters give an excellent reproduction of some features of the measured results, in particular, for  $-F_{12}(\theta)/F_{11}(\theta)$  and  $F_{34}(\theta)/F_{11}(\theta)$ . This might be explained as follows. The larger axis of the particles represents the extraordinary direction that has the larger refractive index. The refractive index used in the calculations is smaller than it should be for the longer axis of particles. This smaller refractive index is then apparently compensated in the particle-size estimation with larger particle lengths.

Although the agreement between the measured  $F_{22}(\theta)/F_{11}(\theta)$  and the calculated function is improved for the estimated parameters with a larger average length/width ratio, we did not find parameters so that  $F_{22}(\theta)/F_{11}(\theta)$  is reproduced accurately. This function is probably sensitive to the exact shape and birefringence of the particles.

In principle, other methods can be used to take the exact shape of the particles into consideration. For example, the discrete-dipole-approximation method (e.g., Refs. 30–32) can be used to analyze the measured data. However, this method is much more time-consuming, and standard programs based on this method are unable to incorporate birefringence. At present, work on a new integral equation program capable of handling birefringence is in progress.

## 9. Conclusions

With our experimental setup we have measured the entire scattering matrix of randomly oriented rutile particles in water between scattering angles of 15 and 165 deg. The results of these measurements strongly indicate the shape irregularity and the birefringence of these particles, most notably in the matrix element ratios  $F_{22}(\theta)/F_{11}(\theta)$  and  $F_{24}(\theta)/F_{11}(\theta)$ .

It appears that T-matrix calculations for prolate spheroids not incorporating the birefringence of the particles are able to reproduce the shape of the phase function and the angular dependence of most element ratios of the scattering matrix remarkably well, when for the calculations a greater mean length/width ratio is used than is actually determined from TEM measurements.

We thank M. I. Mishchenko for use of the T-matrix code and for his careful and constructive review. The personnel of the Kemira Pigments Research and Physics Laboratories is acknowledged for their kind assistance in preparation of the rutile samples. We also appreciate Kemira Pigments for permission to carry out this research and publish the results. We are grateful to L. B. van den Hoek for performing the calculations that led to the correction function given in Fig. 4. Furthermore we thank J. Bouma for extensive technical support and J. M. M. Tesselaar for constructing the glass basin and cuvette.

## References

1. V.-M. Taavitsainen and J. -P. Jalava, "Soft and harder multivariate modeling in developing the properties of titanium dioxide pigments," *Chemom. Intell. Lab. Syst.* **29**, 307–319 (1995).
2. H. C. van de Hulst, *Light Scattering by Small Particles* (Wiley, New York, 1957).
3. C. F. Bohren and D. R. Huffman, *Absorption and Scattering of Light by Small Particles* (Wiley, New York, 1983).
4. J. -P. Jalava, "Precipitation and properties of TiO<sub>2</sub> pigments in the sulfate process. 1. Preparation of the liquor and effects of iron(II) in isoviscous liquor," *Ind. Eng. Chem. Res.* **31**, 608–611 (1992).
5. H. Schnablegger and O. Glatter, "Simultaneous determination of size distribution and refractive index of colloidal particles from static light-scattering experiments," *J. Colloid Interface Sci.* **158**, 228–242 (1993).
6. H. Volten, J. F. De Haan, J. W. Hovenier, W. Vassen, R. Schreurs, A. Dekker, H. J. Hoogenboom, F. Charlton, and R. Wouts, "Laboratory measurements of angular distributions of light scattered by phytoplankton and silt," *Limnol. Oceanogr.* **43**, 1180–1197 (1998).
7. M. I. Mishchenko, "Light scattering by size-shape distributions of randomly oriented axially symmetric particles of a size comparable to a wavelength," *Appl. Opt.* **32**, 4652–4666 (1993).
8. J. W. Hovenier and C. V. M. van der Mee, "Fundamental relationships relevant to the transfer of polarized light in a scattering atmosphere," *Astron. Astrophys.* **128**, 1–16 (1983).
9. J. W. Hovenier, H. C. van de Hulst, and C. V. M. van der Mee, "Conditions for the elements of the scattering matrix," *Astron. Astrophys.* **157**, 301–310 (1986).
10. J. W. Hovenier and C. V. M. van der Mee, "Testing scattering matrices, a compendium of recipes," *J. Quant. Spectrosc. Radiat. Transfer* **55**, 649–661 (1996).
11. M. W. Ribarsky, "Titanium dioxide (TiO<sub>2</sub>) (rutile)," in *Handbook of Optical Constants of Solids*, E. D. Palik, ed. (Academic, New York, 1985), pp. 795–804.
12. G. M. Hale, "Optical constants of water in the 200-nm to 200- $\mu$ m wavelength region," *Appl. Opt.* **12**, 555–563 (1973).
13. J. -P. Jalava, V.-M. Taavitsainen, L. Lamberg, and H. Haario, "Determination of particle and crystal size distribution from turbidity spectrum of TiO<sub>2</sub> pigment by means of T-matrix," *J. Quant. Spectrosc. Radiat. Transfer* **60**, 399–409 (1998).
14. J. W. Hovenier, "Measuring scattering matrices of small par-

- ticles at optical wavelengths," in *Light Scattering by Nonspherical Particles*, M. I. Mishchenko, J. W. Hovenier, and L. D. Travis, eds. (Academic, San Diego, Calif., 1999), pp. 355–365.
15. P. Stammes, "Light scattering properties of aerosols and the radiation inside a planetary atmosphere," Ph.D. dissertation (Free University, Amsterdam, The Netherlands, 1989).
  16. F. Kuik, P. Stammes, and J. W. Hovenier, "Experimental determination of scattering matrices of water droplets and quartz particles," *Appl. Opt.* **30**, 4872–4881 (1991).
  17. F. Kuik, "Single scattering of light by ensembles of particles with various shapes," Ph.D. dissertation (Free University, Amsterdam, The Netherlands, 1992).
  18. S. Sugihara, M. Kishino, and N. Okami, "Backscattering of light by particles suspended in water," *Phys. Chem. Res.* **76**, 1–8 (1982).
  19. E. S. Fry and K. J. Voss, "Measurements of the Mueller matrix for phytoplankton," *Limnol. Oceanogr.* **30**, 1322–1326 (1985).
  20. D. A. Cross and P. Latimer, "Angular dependence of scattering from *Escherichia Coli* cells," *Appl. Opt.* **11**, 1225–1228 (1972).
  21. M. I. Mishchenko, D. W. Mackowski, and L. D. Travis, "Scattering of light by bispheres with touching and separated components," *Appl. Opt.* **34**, 4589–4599 (1995).
  22. K. D. Lofftus, M. S. Quinby-Hunt, A. J. Hunt, F. Livolant, and M. Maestre, "Light scattering by *Prorocentrum micans*: a new method and results," *Appl. Opt.* **31**, 2924–2931 (1992).
  23. G. Mie, "Beiträge zur Optik trüber Medien speziell kolloidaler Metallösungen," *Ann. Phys. (Leipzig)* **25**, 377–445 (1908).
  24. J. E. Hansen and L. D. Travis, "Light scattering in planetary atmospheres," *Space Sci. Rev.* **16**, 527–610 (1974).
  25. D. Miller, M. S. Quinby-Hunt, and A. J. Hunt, "Laboratory studies of angle- and polarization-dependent light scattering in sea ice," *Appl. Opt.* **36**, 1278–1288 (1997).
  26. M. I. Mishchenko and D. W. Mackowski, "Electromagnetic scattering by randomly oriented bispheres: comparison of theory and experiment and benchmark calculations," *J. Quant. Spectrosc. Radiat. Transfer* **55**, 683–694 (1996).
  27. M. I. Mishchenko and L. D. Travis, "Capabilities and limitations of a current FORTRAN implementation of the T-matrix method for randomly oriented, rotationally symmetric scatterers," *J. Quant. Spectrosc. Radiat. Transfer* **60**, 309–324 (1998).
  28. M. I. Mishchenko and L. D. Travis, "Light scattering by polydispersions of randomly oriented spheroids with sizes comparable to wavelengths of observation," *Appl. Opt.* **33**, 7206–7225 (1994).
  29. H. Haario and V. -M. Taavitsainen, *Data Analysis Toolbox for use with Matlab* (ProfMat Oy, Helsinki, Finland, 1997).
  30. E. M. Purcell and C. R. Pennypacker, "Scattering and absorption of light by nonspherical dielectric grains," *Astrophys. J.* **186**, 705–714 (1973).
  31. B. T. Draine, "The discrete-dipole approximation and its application to interstellar graphite grains," *Astrophys. J.* **333**, 848–872 (1988).
  32. K. Lumme, J. Rahola, and J. W. Hovenier, "Light scattering by dense clusters of spheres," *Icarus* **126**, 455–469 (1997).